

## Article

# Measurement and Analysis of Brake and Tyre Particle Emissions from Automotive Series Components for High-Load Driving Tests on a Wheel and Suspension Test Bed

Martin Kupper<sup>1,\*</sup> , Ludwig Schubert<sup>2</sup> , Manfred Nachtnebel<sup>3</sup> , Hartmuth Schröttner<sup>3,4</sup>, Michael Peter Huber<sup>2</sup> , Peter Fischer<sup>2</sup> and Alexander Bergmann<sup>1</sup> 

<sup>1</sup> Institute of Electrical Measurement and Sensor Systems, Graz University of Technology, 8010 Graz, Austria

<sup>2</sup> Institute of Automotive Engineering, Graz University of Technology, 8010 Graz, Austria

<sup>3</sup> Austrian Centre for Electron Microscopy, 8010 Graz, Austria

<sup>4</sup> Institute of Electron Microscopy and Nanoanalysis, Graz University of Technology, 8010 Graz, Austria

\* Correspondence: martin.kupper@tugraz.at; Tel.: +43-316-873-30585

**Abstract:** A current challenge in realising clean road transport is non-exhaust emissions. Important advances regarding measurement systems, including well-defined characterisation techniques, as well as regulation, will be made in the next few years. In this work, we present the detailed results of particle emission analyses, consisting of aerosol (size distribution, particle number (PN), and mass (PM)) and electron microscopy (EM) measurements, under different load conditions on a test bed for a wheel suspension and brakes. Standard tyres and brakes from serial production were tested with a high-load driving cycle, while particle measurements were conducted by gravimetric measurements and with a TSI SMPS, a TSI APS, and a GRIMM OPS. Furthermore, samples were analysed by electron microscopy. A bimodal particle size distribution (PSD) was obtained with an SMPS, with peaks at 20 nm and around 400 nm. The results of an EM analysis of >1400 single particles from the electrostatic sampler match the PSD results. The EM analysis also showed ultrafine particles, mainly containing O, Fe, Si, Ba, Mg, and S, and also fractal particles with high-C fractions. Our results suggest, in agreement with the previously published literature, that particulate emissions are related to the brake disc temperature and occur in significant amounts above a threshold temperature.

**Keywords:** non-exhaust emissions; brake wear aerosol; particle measurement; ultrafine particles; electron microscopy



**Citation:** Kupper, M.; Schubert, L.; Nachtnebel, M.; Schröttner, H.; Huber, M.P.; Fischer, P.; Bergmann, A. Measurement and Analysis of Brake and Tyre Particle Emissions from Automotive Series Components for High-Load Driving Tests on a Wheel and Suspension Test Bed. *Atmosphere* **2024**, *15*, 430. <https://doi.org/10.3390/atmos15040430>

Academic Editors: Kenichi Tonokura, Yan Zhang, Volker Matthias and Jana Moldanova

Received: 15 February 2024

Revised: 15 March 2024

Accepted: 27 March 2024

Published: 29 March 2024



**Copyright:** © 2024 by the authors. Licensee MDPI, Basel, Switzerland. This article is an open access article distributed under the terms and conditions of the Creative Commons Attribution (CC BY) license (<https://creativecommons.org/licenses/by/4.0/>).

## 1. Introduction

In the last few decades, efforts to limit air pollution have been successful. In Europe, the concentrations of pollutants in the air are constantly decreasing, but air pollution in urban areas is still a major health concern [1]. The vast majority of Europeans living in cities are exposed to particulate matter (PM) levels above the WHO limit [2]. As particulate exhaust emissions from transport, the largest emitter in recent decades, are nowadays heavily regulated, other sources come to the fore. Particulate emissions from brake wear (BW) and tyre wear (TW), together with road surface wear, are known as non-exhaust particle (NEP) emissions. NEPs have been studied for decades, as they contribute to at least half of the ambient PM that can be attributed to transport [3] and can reach up to 90% [4]. The contribution of BW to NEP emissions ranges from approximately 16 to over 50 per cent [3,5,6], and the contribution of TW to NEP emissions ranges from approximately 5 to over 30 per cent [6,7]. An almost equal contribution of NEP and exhaust emissions to total traffic-related PM<sub>10</sub> was already known 10 years ago [5], and the ever-increasing and eventually overwhelming proportion of electrified vehicles (EVs) will continuously increase this fraction as the emission of NEPs is also relevant for EVs [8–10]. As a consequence of these trends, initial regulatory efforts resulted in a harmonised procedure for the laboratory measurement of brake emissions for

light-duty vehicles, specified in Global Technical Regulation (GTR) 24 of the UNECE. The latest European emission legislation, EURO 7, relates to GTR 24 and additionally introduces emission limits for BW and abrasion limits for TW, as was announced, for instance, by a press release from the European Commission in December 2023 [11].

The current research on NEPs covers measurement techniques, the characterisation of emissions, and fundamental formation mechanisms. The Euro 7 legislation-compliant method for brake wear (BW) particles is one area of research. The Particle Measurement Programme (PMP) informal working group of the UNECE coordinated a global interlaboratory study [12,13] to assess and compare possible established measurement setups [14]. This ultimately led to the definition of UN GTR 24, which was adopted for Euro 7. The emissions of a single brake have to be measured on a fully encapsulated brake test bed following the newly defined “WLTP-Brake” cycle. The harmonised methodology ensures the representative and precise measurement of the particle mass and particle number (PN). In this context, the measurement of the Total Particle Number (TPN), in addition to the engine-emissions-established Solid Particle Number (SPN), was considered relevant [15]. Comprehensive studies on NEP measurement and sensor techniques have identified two main principles for NEP measurement [16]. According to UN GTR 24, PM<sub>10</sub> and PM<sub>2.5</sub> emissions should be determined by gravimetric filter weighing, with two separate filter holders and cyclones for each cut-off diameter. The PN should be measured by means of TPN<sub>10</sub> and SPN<sub>10</sub>, using PN sensors with a lower cut-off diameter (50% detection efficiency) at 10 nm electrical mobility diameter. This involves PN pre-classifiers, such as a 2.5 µm cyclone to remove larger particles, a dilution system with one or more dilution stages, an optical Particle Number Counter (PNC), and a volatile particle remover if the SPN is measured.

Efforts are also being made to explore new sampling technologies for Real Driving Emissions (RDE) of BW particles to quantify on-road emissions in traffic and challenge the defined test-bed procedure of GTR 24 for its representativeness. The brake temperature, that is, the brake disc temperature (BDT), is recognised as impacting PM and PN brake emissions [3,10], particularly after surpassing a critical threshold temperature, where volatile particles can be released with a mode at 10 nm to 30 nm [14,17]. Defining cooling conditions on the test bed keeps the brake temperature well under this threshold. In reality, the temperature behaviour of a brake system is directly impacted by various factors, including ambient conditions, changes in elevation, driving habits, vehicle design, and recuperation strategy. Therefore, assessing the inherent cooling characteristics of a particular vehicle’s brakes plays a pivotal role in evaluating its actual BW emissions [18,19].

The progress for tyre wear (TW) is not as advanced as for BW, although it is the source of ~5% of total ambient PM. While only a small fraction (2% to 5%) becomes airborne, the majority of TW contributes to global microplastic contamination [7,20]. For this reason, the UNECE established the Task Force on Tyre Abrasion (TFTA) in 2022 to develop a standardised test procedure for the reproducible measurement of TW. The vehicle convoy method on public roads and the indoor drum dynamometer method are currently under evaluation. However, the current objective is limited to a method for measuring TW by weight loss in order to quickly achieve a reduction in microplastics on European roads. Whether a method for determining airborne tyre emission particles will also be developed in the future remains to be seen and is currently only the subject of research projects [7,21–23].

The measurement of NEPs is also a challenge at the sensor level, as NEP aerosols have a very heterogeneous composition and cover a broad size range, as shown by the results of this work, in accordance with the literature [3,20]. This is in contrast to the exhaust particle measurement method established in the automotive environment decades ago, where only soot particles are measured [24,25]. The PNCs that are typically used for SPN and TPN measurements are Condensation Particle Counters (CPCs) [9,13,18], which are known to have a material dependency [26–28]. Electrical spectrometers, which are often used for size distribution measurements, depend on the effective particle density, which

is generally unknown and differs for particles of different materials. This density is also strongly affected by the brake pad formulation and particle size [16]. The topic of sensors for reliable NEP detection should be considered for future research efforts.

In this work, we present the results of a feasibility study of NEP aerosol measurements and EM analysis conducted on a wheel and suspension test bed with a closed ventilation system. A fully automated 200 s high-load drive cycle was repeated a total of 1100 times in sets of 20 consecutive repetitions. The drive cycle does not represent on-road driving behaviour, as equivalent driving manoeuvres cannot be realised with a vehicle and a driver; it was designed to maximise wear and NEP emissions. Details on the test cycle can be found in Appendix B. We measured the NEPs for size distribution and number concentration with aerosol instrumentation at various sampling positions to be able to qualitatively assess the method. We also characterised NEPs with EM for size distribution and chemical composition from a filter sample and dedicated samples from an electrostatic sampler. The total wear was assessed by gravimetric methods.

## 2. Materials and Methods

All measurements were carried out on a wheel and suspension test bed, which is described in detail below. It is a component test bench for any complete wheel carrier, including the complete brake system, rim, and tyre. It is equipped with a closed ventilation system, due to which it is possible to measure the total particle emissions from the components on the test bed. Particle measurements were carried out using aerosol instrumentation and through the electron microscopy (EM) analysis of filters and specific samples.

### 2.1. Wheel and Suspension Test Bed

The test setup, as illustrated in Figure 1a, involves a steerable steel drum designed to apply a specific skew angle. The drum is coated with an abrasion-resistant layer, which is based on a real road surface with similar friction values. Additionally, the test bed is equipped with both a master cylinder, regulating brake pressure, and a hydraulic cylinder, controlling vertical forces. Two motors, one inside the drum and another dedicated to wheel propulsion, have the capability to regulate drive torque and induce a specific slip on the tyre.

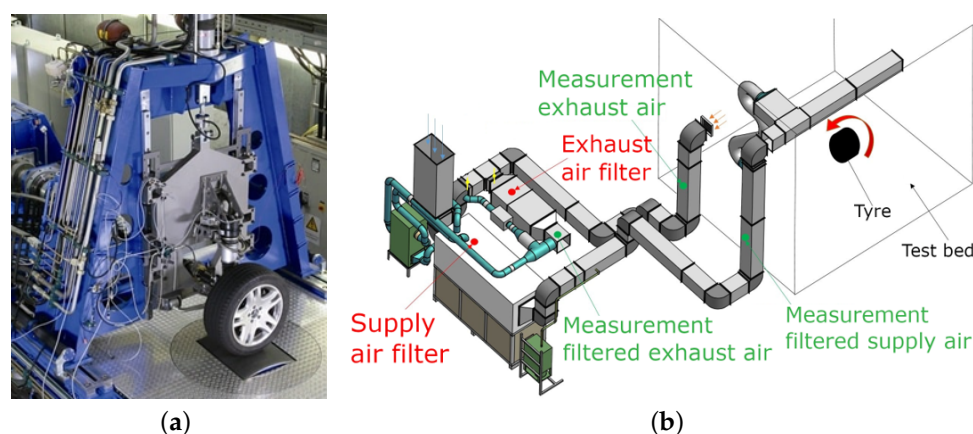


**Figure 1.** The visualisation of the wheel and suspension test bed at the Institute of Automotive Engineering at the Graz University of Technology. (a) A CAD rendering of the test bed. (b) Schematics of the ventilation with the sampling positions indicated in green and the filter positions in red.

For the test programme described below, a front axle chassis of a passenger car was mounted on the test bed. The entire car had a weight of 2781.5 kg. The tyres used were Continental ContiSportContact 5 summer tyres, with the specifications 255/45 R22 107 XL. The composition of the brake pads was unknown, whereas the brake discs utilised were of grey iron construction.

A special characteristic of the test bed is the closed ventilation system, shown in Figure 1b. Intake air with a volume flow of  $2707 \text{ m}^3 \text{ h}^{-1}$  from the environment is led through the supply

air filter in a continuous flow and passed into the measuring room via several ventilation outlets. The exhaust air is displaced through one ventilation opening and led through the exhaust air filter before being ventilated into the environment. The filters are described in the “Aerosol Measurement” Section.

### 2.2. Test Programme

The basis of the test programme was a well-defined high-load cycle of 200 s, which was fully automated and consecutively repeated in sets of 20 repetitions. Each set was followed by a pause to cool the components, change the measurement position of the aerosol instrumentation, and, if necessary, perform service and control work. On a single test day, 5 sets were completed; the brake pads and tyres were exchanged for unused ones after each day, and the tyre and rim were balanced properly. Brake pads and tyres were weighed before and after use. These filters were also weighed before and after installation. The tests were carried out over 11 consecutive days, resulting in a total of 1100 repetitions of the 200 s cycle. New air filters were installed for the supply and exhaust air of the test bed’s ventilation system for the test programme. The filters are detailed in the “Aerosol Measurement” Section.

The test programme was intended to exceed the maximum possible material stress that occurs under real driving conditions to test the robustness of the components, maximise wear, and thus maximise NEP emissions. Equivalent driving manoeuvres cannot be realised with a vehicle and a driver.

The test cycle was fully defined by time-dependent set values for roller drive speed, drive torque, driving force, braking pressure, wheel vertical force, wheel vertical position, lateral force, suspension strut travel, pivot angle of the roller, and airstream. See Appendix B for the time-dependent set values of drive speed and acceleration, torque, slip angle, and brake pressure. A table with representative test cycle parameters is available in the online Supplementary Material. Selected measured parameters of the test cycle can be seen in Figure 2b–e.

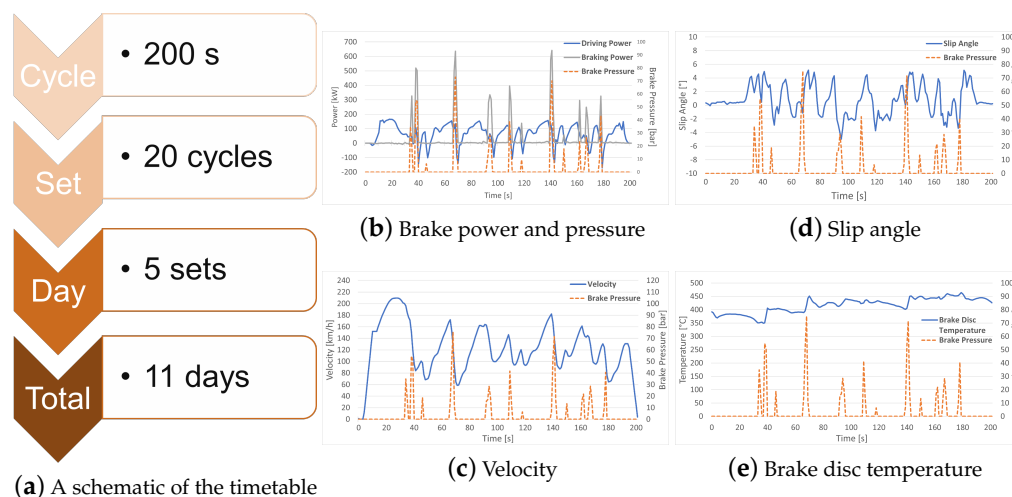


**Figure 2.** A representation of the used test programme on the wheel and suspension test bed. (a) The structure of the programme and (b–e) selected time-dependent parameters of the test cycle; see Appendix B for details.

During each cycle, the test-bed operating system measured and recorded the following parameters: time, suspension strut travel, slip angle, wheel vertical force, roller drive speed, driving force, pressure in the brake cylinder, flywheel torque, ambient temperature, wheel vertical position, drive torque, braking torque, lateral force, BDT, tyre tread temperature (left, middle, and right), and driven distance.

### 2.3. Aerosol Measurements

We measured the PN concentration and the particle size distribution (PSD) of ultrafine and larger particles, determined the airborne PM by gravimetric methods, and collected samples of particles for electron microscopy analysis. Aerosol measurements were carried out at the three measurement positions indicated in Figure 1b in green with all instruments. Measurements were also taken inside the test bed with the APS described below and a custom-made electrostatic sampling device for electron microscopy analysis.

For the aerosol measurements, a TSI 3775 Condensation Particle Counter (CPC) was used to measure the PN concentrations of ultrafine particles (UFPs). According to the manufacturer's specifications, the TSI 3775 fully detects particles down to a diameter of roughly 10 nm. It has a detection efficiency of 50 % at 4 nm and 10 % at roughly 1.5 nm. In combination with a TSI 3081 Differential Mobility Analyser (DMA) and a TSI 3080 electrostatic classifier, equipped with a TSI 3077 X-ray source, a Scanning Mobility Particle Sizer (SMPS) setup was formed to measure the PSD of UFPs. For larger particles, a TSI 3321 Aerodynamic Particle Sizer (APS) was used, which allows for the measurement of the PN concentration and PSD for aerosol particles in the size range from 0.37  $\mu\text{m}$  to 20  $\mu\text{m}$ . Additionally, a Grimm Dustdecoder 11-D (Optical Particle Spectrometer—OPS), which measures the PN concentration and PSD for aerosol particles in the size range from 0.253  $\mu\text{m}$  to 35.15  $\mu\text{m}$ , was available, but its usage was limited due to a malfunction that occurred. With the knowledge of the PSD, the PM concentration can be estimated by assuming a mean particle density.

Samples for the electron microscopy analysis were collected by a custom-made electrostatic sampler, with four deposition stages operated at different voltages to separate different mobility diameters. Details can be found in Appendix A. The set voltages were 200 V, 400 V, and 800 V, as well as one at 0 V potential for reference. For singly charged particles, this would mean a deposition of particles up to a mobility diameter of 62 nm for 200 V, 91 nm for 400 V, and 136 nm for 800 V. See Appendix A.2 for the theoretical details.

As described above, new filters for fresh and exhaust air in the test-bed ventilation system were installed before testing and were used for the gravimetric analysis of the airborne PM. The used filters were Kappa Wavebionix® with a filtration efficiency of 97.2 % at 28 nm, according to the manufacturer's data sheet.

### 2.4. Electron Microscopy Analysis

For EM analysis, two types of samples were available. Firstly, the exhaust air filter was analysed, and secondly, particles were sampled by an electrostatic sampler inside the test bed. The dimensions of the electrostatic deposition plates in the sampler match the possible sample sizes of the EM devices and were analysed directly. For the exhaust air filter, EM samples had to be prepared according to the method described in [29]. The filter was cut open, and particles were removed by shaking the filter with the opening facing downwards over a previously cleaned container. A small, representative portion of the collected material was carefully placed into a glass and positioned under carbon tape stripes with the adhesive side facing downwards. CO<sub>2</sub> was blown from the vessel to swirl the particle material, resulting in an assumed representative distribution of particles on the adhesive carbon tape. The tape stripes were then used as samples for EM analysis.

All samples were investigated using automated particle analysis through the combination of Scanning EM (SEM) and Energy-Dispersive X-ray Spectroscopy (EDX). Thus, a Zeiss Sigma 300 VP, which was equipped with an Oxford X-max N80 EDX detector, was used. To perform automated acquisition and particle analysis, the Oxford built-in Aztec 3.4 software was utilised. Appropriate image thresholding of acquired Back-Scattered Electron (BSE) images was used for segmentation between the background (substrate) and particles. Image stacking was performed to analyse sufficiently large areas to obtain the particle counts stated in the next section. For the stated particle sizes in the PSD, the equivalent circular diameter (ECD) was chosen, which was calculated from the measured projected particle areas.

### 3. Results

#### 3.1. Gravimetric Measurements

To assess the total wear mass, the used brake discs, brake pads, and tyres were weighed before installation in the test bed and again after removal. The results can be seen in Table 1. In total, 1345 g of mass was removed during the test drives, of which 70 % came from the tyres.

**Table 1.** Measured weight differences.

Component	Weight Difference
Brake Disc Total	−71 g
Brake Pad Total	−306 g
Tyre Total	−968 g
Total Wear	−1345 g
Fresh Air Filter	12 g
Exhaust Air Filter	338 g

The air filters from the ventilation system were also weighed before and after installation. For the fresh air filter, a small weight change of 12 g was determined, while the exhaust air filter gained 338 g of mass. Therefore, 25.13 % of the total wear mass was found in the exhaust air filter.

In total, 6799 km was driven in the test campaign, which means that at least  $198 \text{ mg km}^{-1}$  of airborne PM was emitted. The particle emissions have been found to be very repeatable, no substantial differences have been observed between separate sets.

#### 3.2. Size Distribution Measurements

The data measured with the SPMS and APS were combined to show the PSD over the total covered range. The device combination was used at sampling positions for filtered supply air, exhaust air, and filtered exhaust air in the ventilation system of the test bed, as indicated in green in Figure 1b. The APS and the Grimm device were also used for measurements inside the measurement room of the test bed. The results can be seen in Figure 3. It was not possible to acquire reliable PSD data with the Grimm device due to a malfunction.

The presented study was conducted to investigate the feasibility of particle measurements on a wheel and suspension test bed; thus, the presented PSD data can provide information on the general trends and shapes of the distributions. The presented particle sizes obtained with the used instruments are shown as the respective equivalent diameters; qualitative comparability is nonetheless provided. The used equivalent diameters are the mobility diameter for the SMPS, the aerodynamic diameter for the APS, and the equivalent circular diameter for EM. The presented normalised concentrations ( $\text{dN}/\text{dlogD}_p$ ) increase the comparability of measurements with different widths of the size bins, but the concentrations are several orders of magnitude larger than measured. The PSD with non-normalised concentrations, with the preserved order of magnitude of the measurements, can be found in Appendix C.

As described above, PM values can be derived from the PSD by assuming a mean particle density. As the mean density of the measured particles is not known, a calculation with an assumed density of  $2.2 \text{ g cm}^{-3}$  [30,31] helps to contextualise the detected amounts. We used the same value for all sizes and assumed spherical particles with the size of the measured equivalent diameters. The estimated PM values ranged from  $300 \text{ } \mu\text{g m}^{-3}$  to  $400 \text{ } \mu\text{g m}^{-3}$ , with maximum values at  $450 \text{ } \mu\text{g m}^{-3}$ . These values will give an estimation regarding the order of magnitude.

As described above, through the EM analysis of the exhaust air filter, it was possible to determine the PSD, which can be seen superimposed on the exhaust air measurements performed with the SMPS and the APS in Figure 3c.

In the filtered supply air, only measured the SMPS was able to measure a PSD due to the small sizes, as can be seen in Figure 3a. The thus-induced particle background on the

order of  $10^2 \#/\text{cm}^3$  is orders of magnitude below the measured values in the exhaust air flow and was not taken into account in further evaluations.

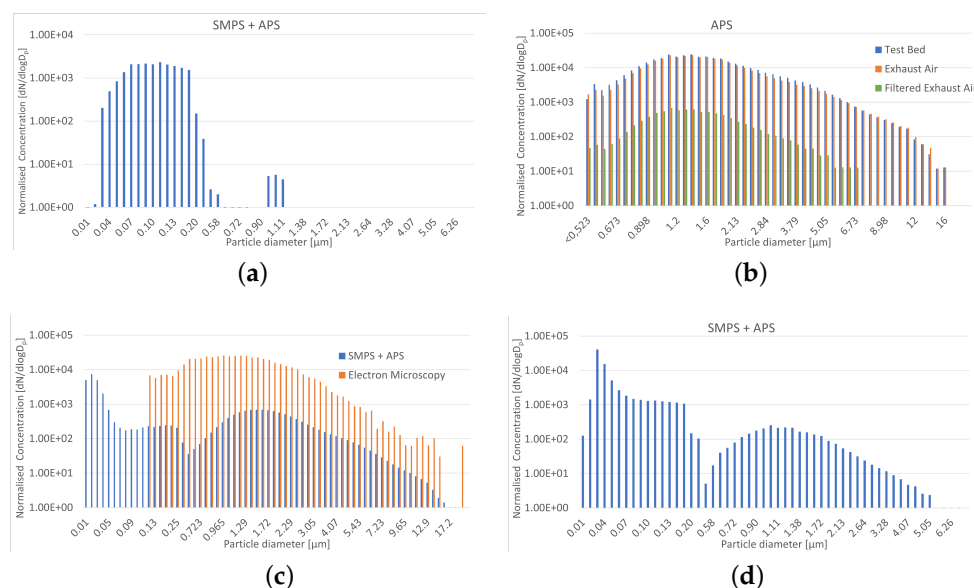


**Figure 3.** PSDs for different sampling positions (see Figure 1b), measurements, and instruments for qualitative comparison. Different equivalent diameters were used for the different instruments. Plots with non-normalised concentrations can be found in Appendix C. (a) PSDs measured in filtered supply air with the SMPS and APS. (b) A comparison of APS measurements for different sampling positions. (c) A comparison of PSDs measured in exhaust air with three different techniques. (d) PSDs measured in filtered exhaust air with the SMPS and APS.

Figure 3b shows data from APS measurements at different sampling positions; the shape of the distribution does not change, while the concentrations differ. A similar behaviour can be observed by comparing Figure 3c,d; the shape of the distribution in the filtered exhaust air is very similar to the one measured in the exhaust air, but the concentrations differ.

### 3.3. Particle Number Concentration Measurements

From the raw data from single cycles, as exemplified in Figure 4a, it can be recognised that the PN concentration becomes comparable between cycles from the third cycle onwards. The analysis of BDT measurements showed that the BDT also levels off and is comparable from the third cycle onwards. Thus, we focussed on analysing the data after the bedding-in period of the first two cycles of each set.

The PN concentration changes in relation to braking events and changes in the BDT, as can be seen in Figure 4b. A linear scale was chosen for the PN concentration in this visualisation to make the changes more visible. Each braking event is followed by an increase in temperature, with the extent depending on the brake pressure. For strong braking events, the increase in temperature is then followed by an increase in the PN concentration. The BDT is very high compared to what can be expected from actual driving or heavy braking; this will be discussed in more detail later.

Comparing the data from the filtered and unfiltered exhaust air shows that the exhaust air filter reduces the UFP concentration by one order of magnitude; thus, roughly 90% of the UFP PN concentration is captured in the filter.

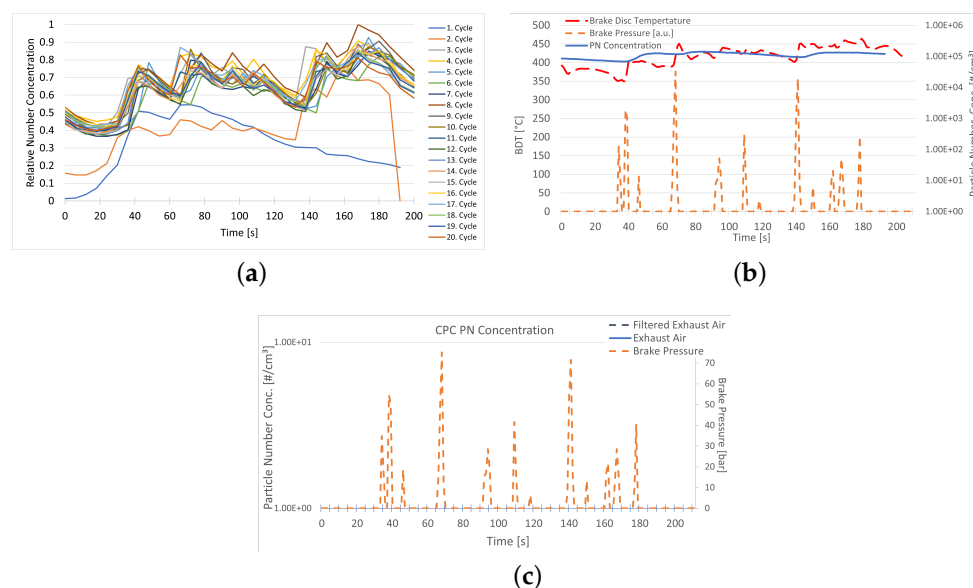


**Figure 4.** Plots of the PN data for different sampling positions and measurements. **(a)** Raw relative PN concentration data from one set (20 cycles). **(b)** Mean CPC PN concentration and brake BDT data from one set measured in exhaust air on a linear scale. Braking events are indicated by brake pressure data in arbitrary units to illustrate the correlation with the temperature and PN concentration. **(c)** CPC PN concentration data on a logarithmic scale for a comparison of unfiltered and filtered exhaust air.

### 3.4. Electron Microscopy Measurements

All samples were scanned automatically, and the single particles were analysed for size and composition. For samples taken from the exhaust air filter, the PSD can be seen in Figure 3c, along with the corresponding PSD acquired with aerosol instrumentation. The PSD from the different deposition stages of the electrostatic sampler can be seen in Figure 5a, and the corresponding total numbers are listed in Table 2. The found particle sizes in terms of ECDs do not match the expected sizes according to the calculations of the mobility diameter. As shown in Figure 5a, the shape of the PSD is very similar for all three plates, and the 0 V reference plate was found to be particle-free. The separation of particles between the deposition stages was instead determined by structural properties, as indicated in the exemplary EM images in Figure 5, and composition, as described below. The aggregates seen in Figure 5b from the 200 V plate are comparatively small, the largest were found on the 400 V plate and are shown in Figure 5c, while the particles in Figure 5d, from the 800 V plate, are similar to soot particles.

**Table 2.** Number of particles determined by EM single-particle analysis.

Location	Number of Particles
0 V deposition voltage	0
200 V deposition voltage	7371
400 V deposition voltage	6374
800 V deposition voltage	2758
Total	16,503

The particle composition was analysed by EDX of single particles. The results can be seen in Table 3. The mass fractions were calculated from the obtained single-particle spectra using the factory-calibrated standardisation process from the used instrumentation software AZtec. The proportion of particles containing certain elements differs between the different deposition stages. For example, 88 % of found particles on the 200 V plate contain iron, and the total iron mass percentage was found to be about 10 %, while on the 800 V plate, the number of particles with iron was about 52 %, but the mass percentage was also about 10 %. A similar result can be seen for carbon, where the number of particles

containing carbon was 39 % for the 200 V plate, about 10 % for the 400 V plate, and over 95 % for the 800 V plate, whilst the carbon mass fraction was found to be very similar for all three deposition stages.

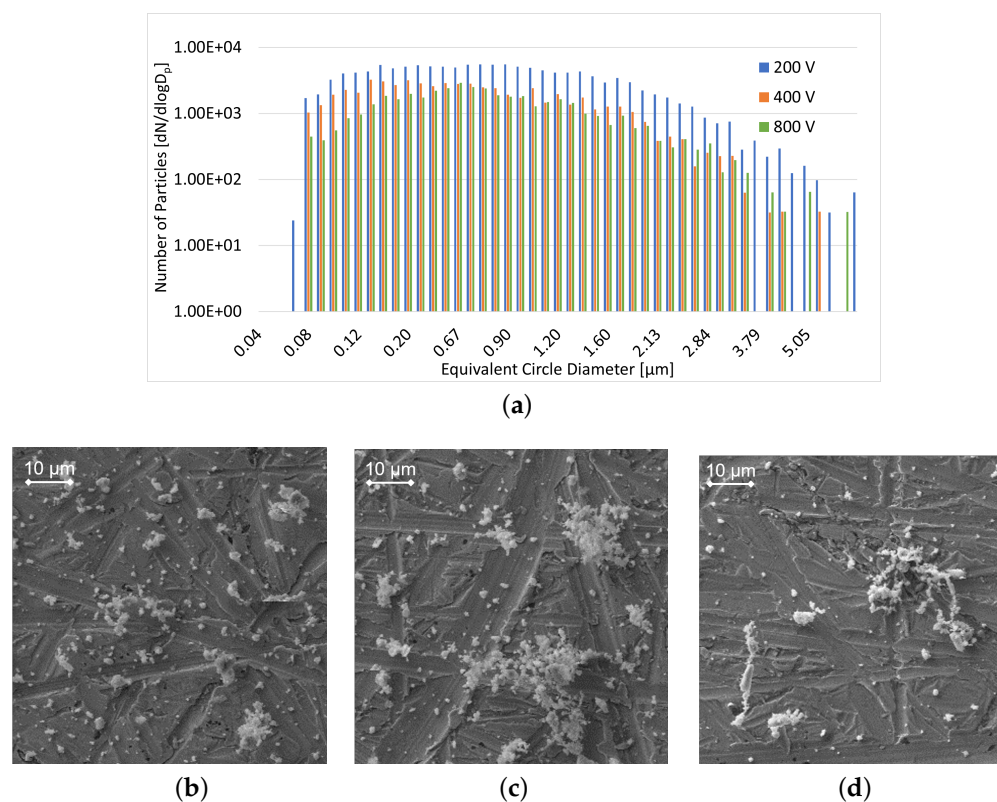


**Figure 5.** The results of the EM analysis. The graph in (a) shows obtained ECDs from the single-particle analysis of the deposition plates. The images in (b–d) show exemplary regions of the deposition plates for different voltages to illustrate the differences in the constitution of the particles found. The results of the composition analysis of the single particles can be found in Table 3. (a) The PSD determined by EM single-particle analysis. Note that the  $y$ -axis is normalised; the figure with absolute concentrations can be found in Appendix C. (b) Particles sampled with 200 V, corresponding to mobility diameters below 62 nm. (c) Particles sampled with 400 V, corresponding to mobility diameters below 91 nm. (d) Particles sampled with 800 V, corresponding to mobility diameters below 136 nm.

As the plates in the electrostatic sampler were made of copper, and the sample tape for the samples from the filter was mainly made of carbon, the results for these elements cannot be attributed to only the particle content. This is due to the small particle size in comparison with the electron beam interaction; with an electron beam, an EDX signal from the substrate is also generated in any measurement. Due to these circumstances and other conditions, such as inhomogeneity and the structure of the particles, the results have to be seen as a semi-quantitative analysis. Nonetheless, as thousands of particles were measured, the analysis provides a valid insight into the mean composition of the particles. If any particles were identified with the composition of the pure substrate, they were automatically disregarded.

**Table 3.** The results of EDX measurements. The substrate material, Cu for the electrostatic sampler and C for the filter, is indicated in grey. The first column gives the fraction of particles found containing the specified element. The second column gives the mass fraction of the specified element in relation to the total analysed mass.

Element	200 V		400 V		800 V		Filter	
	#/%	wt/%	#/%	wt/%	#/%	wt/%	#/%	wt/%
Cu	98.05	36.4	100.00	33.1	99.61	66.9	0.10	1.6
O	94.99	9.2	89.28	7.5	83.73	8.7	95.70	16.9
Fe	88.30	10.2	85.59	8.8	51.57	10.6	38.40	10.4
Si	59.64	3.2	70.52	2.7	41.18	3.1	99.80	1.0
Ba	62.12	4.3	60.30	2.8	33.53	3.8	24.20	2.9
Si	57.94	1.3	50.59	0.9	25.49	1.3	25.80	1.9
Mg	50.70	2.0	61.47	2.2	9.41	0.9	12.80	1.4
C	39.00	19.3	9.88	18.1	96.47	17.2	100.00	70.0
Zr	20.61	1.6	14.24	1.8	6.86	2.3	3.00	1.0
Ca	11.98	0.8	13.07	0.5	4.12	0.6	7.00	0.3
Zn	9.75	3.8	6.20	3.0	4.31	4.2	7.90	1.8
Al	3.90	2.3	6.53	2.4	0.59	0.7	0.60	0.5
K	2.51	0.6	0.84	0.4	1.18	1.7	0.40	0.5
Cl	1.39	0.6	1.34	0.3	4.51	0.6	0.04	0.3
Cr	0.56	1.2	3.18	1.6	0.20	1.0	0.30	0.9
Br	0.56	0.7	1.01	1.6	-	-	-	-
P	0.28	1.8	0.34	1.6	0.39	3.2	9.68	0.9
Sn	0.28	2.1	2.18	0.9	-	-	0.30	1.6
Sr	0.28	1.3	-	-	-	-	-	-
Ti	-	-	2.01	1.5	0.59	3.1	0.30	1.1
Pb	-	-	-	-	0.20	3.4	-	-

#### 4. Discussion

From the gravimetric results in Table 1, it can be seen that a considerable amount of wear mass was produced, of which about 25 % was found in the exhaust air filter. The observation that at least a quarter of the total mass loss of the components was found to be airborne must be seen differently. A possible generalisation is not indicated, as the chosen drive cycle targeted the maximised wear of the components in a minimum amount of time to optimise the use of the operation time of the test bed. Driving the cycle with a vehicle is not possible, so this study can give an estimation of the maximum wear emissions from brakes and tyres. Furthermore, the achieved BDTs of around 400 °C are achievable but not commonly anticipated for passenger car usage and are also not accounted for in the WLTP brake cycle [18,19,32], although the critical temperatures for ultrafine particle emissions are considered below or around 200 °C [6,33].

Regarding the distribution of the lost mass of the components in relation to the total mass found in the filter, the results match the latest literature. According to [7], about 2 % to 5 % of TW is airborne. For the measurements presented here, 2 % to 5 % corresponds to 19.36 g to 48.8 g. If this estimated airborne fraction of TW is summed up with the 306 g of mass lost at the brake discs, this adds up to about 338 g found in the exhaust air filter.

It is not possible to draw any conclusions about PM not captured in the filter, as the ventilation system of the test bed is not optimised for aerosol transport and has unknown particle losses. Additionally, the filtration efficiency of the exhaust air filter provided by the supplier unfortunately does not enable any conclusions.

The shape of the obtained PSD is consistent across the different methods and sample positions, as shown in Figure 3, and a good match between the combined SMPS and APS data and the EM data is apparent in Figure 3c. The same behaviour is also represented by the non-normalised data, as can be seen in Figure A3. Again, it is stated here that the sizes compared are from different instruments and are given in different equivalent diameters. The PSD shows a bimodal distribution, with one distinct peak in the UFP region around 20 nm and around 400 nm. Most likely, the bimodal shape does not represent the real distribution.

The aberration from 250 nm to 723 nm is very likely due to the transition region between the instruments, where the SMPS shows deviations when coming closer to its upper size limit of around 1 µm and the APS to its lower size limit. This is also supported by the EM size distribution, which does not match the descent in this region.

Comparing the exhaust air data to the filtered exhaust air, the shape of the PSD is conserved, but the PN is reduced by over an order of magnitude. The remaining PN concentration in the ventilated air was at about ambient levels.

Interestingly, the comparison of the APS data at different measurement positions, shown in Figure 3b, shows almost the same data for the measurement inside the test bed and the exhaust air measurement position, before the filter. This indicates that the emerging aerosols in the measurement chamber are transported relatively efficiently through the ventilation system. But it is not known how these aerosol particles compare to RDE-NEPs, nor how representative they are for NEPs in general.

The behaviour of the obtained PN data matches the observations of BW emissions in the literature [6,30,33] that particles are observed in significant quantities after the BDT exceeds a threshold temperature. We furthermore observed that the level of particle emissions was repeatable and constant in terms of the PSD and PN in our measurements from the third cycle on, after the BDT reached temperatures around 400 °C. This behaviour is illustrated in Figure 4a and was observed for every measured set. For a possible future follow-up measurement campaign, a separation of the SPN and TPN would be of interest.

Because of the given repeatability of the concentrations, the calculation and analysis of mean values are justified. We neglected the first two cycles of each set for the calculation of mean values. In Figure 4b, the exemplary mean values of the PN concentration measured with the TSI 3775 and the BDT from one set are shown. The UFP PN concentration in the exhaust air flow reaches overall considerably high values on the order of  $10^5 \text{ \#/cm}^3$ . A dependence on the BDT can be observed, which is linked to the brake pressure. Stronger braking events, e.g., around second 40 or 70, cause a distinct increase in the BDT, which is then followed by an increase in the PN concentrations with a few seconds' delay. Smaller braking events also cause a change in the BDT but do not cause a clear increase in the PN concentration.

The EM results from the samples drawn with the electrostatic sampler were not as expected. The PSDs from all three deposition plates show the same shape with decreasing numbers, as can be seen in Figure 5a. A total of 44.7% of all particles were found on the 200 V plate, 38.6% on the 400 V plate, and 16.7% on the 800 V plate. From an inspection of the EM images of the three plates, a qualitative difference between the deposited particles on the different plates was observed. On the 200 V plate, there were rather compact particles; on the 400 V plate, there were larger, mesh-like particles; and on the 800 V plate, there were predominantly fractal particles. Although it cannot be verified whether the agglomerates formed in the aerosol phase or at the substrate, the differences in the found structures were noticeable.

Differences between the deposited particles on the different deposition plates can also be seen in the EDX analysis in Table 3. Oxygen is the only element that was found in the majority of particles, irrespective of the sample. In the comparison of the particles from the three electrostatic sampling plates, it was found that iron was present in most particles on the 200 V plate and 400 V plate, but significantly less was on the 800 V plate, although the mass fraction for iron is comparable. For magnesium, the number and the mass fraction are similar for the 200 V and 400 V plates but very different for the 800 V plate. For carbon, the case is particularly peculiar when combined with the observation of fractal particles on the 800 V plate, as almost all of the particles found contain carbon. This is not the case for the other two plates, although the mass fraction is again comparable.

As the separation between the different deposition stages was intended to be based on the mobility diameter, it can be assumed that the deposited particles, which have similar PSDs in terms of ECDs, have different densities. This would support the assumption that agglomerates were already formed in the aerosol phase.

The separation of particles into BW and TW by tracer materials was not possible, as tracer materials for BW (e.g., iron, copper, lead, and calcium [3]) were found in the vast

majority of particles. This could be interpreted in two ways. First, the airborne particles in these measurements were predominantly BW particles. Alternatively, the collected particles could be secondary particles or agglomerates from all primary particle-emitting sources in the test-bed measurement chamber. Assuming the first thesis, it could also explain the peculiar match of the collected PM in the exhaust air filter to the mass loss of the brake pad and brake discs, as listed in Table 1. However, based on current knowledge and the available data, this cannot be verified or falsified.

The here-presented efforts must be contextualised as a feasibility study to measure particle emissions on a wheel and suspension test bed with a closed ventilation system. For future experiments, it is recommended to use a housing around the wheel and brake, similar to that defined for the measurement of brake emissions [13,34], with characterised losses and a well-defined flow profile. For better sourcing of the particle fractions, tyres, brake pads, and brake discs with dedicated tracer materials should be used. Aerosol instrumentation for UFPs should be used along with dilution systems in order to operate in the ideal detection range. Additionally, the sampling for EM analysis should be optimised in terms of the flow design, and the deposition voltages should cover a wider range.

## 5. Conclusions

Particle measurements were carried out on a wheel and suspension test bed equipped with a closed ventilation system for high-load driving scenarios, using an SMPS and an APS for PSD measurements and a CPC for UFP concentration measurements. Samples were taken for EM analysis by means of a custom-made electrostatic sampler.

Our results are coherent for all the utilised measurement and analysis techniques. The exhaust air filter collected approximately  $\sim 25\%$  of the total mass loss of the wear components, indicating predominant emissions from BW. The analysis of the airborne particles showed PN concentrations around  $120 \text{ k\#/cm}^3$  to  $140 \text{ k\#/cm}^3$  in the exhaust air flow with a PSD with one distinct peak in the UFP region around  $20 \text{ nm}$  and considerable PN concentrations below  $10 \mu\text{m}$ . It was found that the airborne particle concentrations are strongly linked to the BDT. The PSD was found to be consistent among the measurement chamber, the exhaust air flow, and the filtered exhaust air flow.

The PSD obtained with EM single-particle analysis of the samples drawn with the electrostatic sampler inside the measurement chamber matches the PSD from the aerosol instruments, and the PSD found in the exhaust air filter is also consistent. The EM analysis of the samples for different mobility diameters surprisingly showed the same PSD shape for all plates, though differences in the constitution and chemical composition of the particles were observed. The EDX analysis furthermore revealed a substantial fraction of metal compounds. The source attribution of the particles based on composition was not possible, as the majority of particles contained a mix of tracer materials from BW, TW, and organic compounds.

For further investigations of wear particles on a wheel and suspension test bed, it is recommended to use a housing with a defined air flow and dilution factor around the wheel and brake for ideally controlled measurement parameters. The sampling position inside the measurement chamber should be varied and, if necessary, optimised. For the PN measurements, the separation of the SPN and TPN would be of interest. Further investigations with electrostatic samplers and EM analysis should cover a wider range of deposition voltages and use sampling plates made of a material that is not expected to be found in NEPs. Future investigations should also cover realistic driving conditions and assess whether the method of measuring NEP emissions on the wheel and suspension test bed is feasible.

**Supplementary Materials:** The following supporting information can be downloaded at <https://www.mdpi.com/article/10.3390/atmos15040430/s1>: Table S1: Selected time dependent set parameters of the test bed from the 200 s test cycle.

**Author Contributions:** Conceptualisation, P.F., M.K. and H.S.; methodology, M.K., M.N., H.S. and P.F.; validation, M.K., H.S. and A.B.; formal analysis, M.K. and M.N.; investigation, L.S. and M.N.; resources, A.B. and P.F.; data curation, L.S., M.N. and M.K.; writing—original draft preparation, M.K.; writing—review and editing, M.K., L.S., M.N., H.S., M.P.H., A.B. and P.F.; visualisation, M.K.; supervision, M.K., A.B. and P.F. All authors have read and agreed to the published version of the manuscript.

**Funding:** The publication was supported by the TU Graz Open Access Publishing Fund.

**Institutional Review Board Statement:** Not applicable.

**Informed Consent Statement:** Not applicable.

**Data Availability Statement:** The data presented in this study are available in Table S1.

**Acknowledgments:** The authors thank the organising team of the TAP conference in Gothenburg 2023 for the possibility to submit manuscripts of accepted conference contributions to the Special Issue “Transport Emissions and Their Environmental Impacts” of MDPI’s *Atmosphere*. Open Access Funding by the Graz University of Technology.

**Conflicts of Interest:** The authors declare no conflicts of interest.

## Abbreviations

The following abbreviations are used in this manuscript:

APS	Aerodynamic Particle Spectrometer
BDT	Brake disc temperature
BW	Brake wear
CPC	Condensation Particle Counter
DMA	Differential Mobility Analyser
ECD	Equivalent circular diameter
EDX	Energy-Dispersive X-ray Spectroscopy
EM	Electron microscopy
GTR	Global Technical Regulation
OPS	Optical Particle Spectrometer
NEP	Non-exhaust particle
PM	Particulate matter
PN	Particle number
PSD	Particle size distribution
RDE	Real Driving Emissions
SMPS	Scanning Mobility Particle Sizer
SPN	Solid Particle Number
TPN	Total Particle Number
TW	Tyre wear
UFP	Ultrafine particle

## Appendix A. Electrostatic Sampler

### Appendix A.1. Description

The sampler has a total length of 40 cm, consisting of a 10 cm inlet and a 24 cm deposition area containing four electrically separated deposition plates with a length of 5 cm, followed by a 6 cm outlet. The parts were manufactured by a 3D printer at the TU Graz. The flow channel in the deposition area has a height of 1 mm and a width of 2.5 cm. The flow through the electrostatic sampler was constant at  $1 \text{ L min}^{-1}$ , provided by an membrane pump downstream.

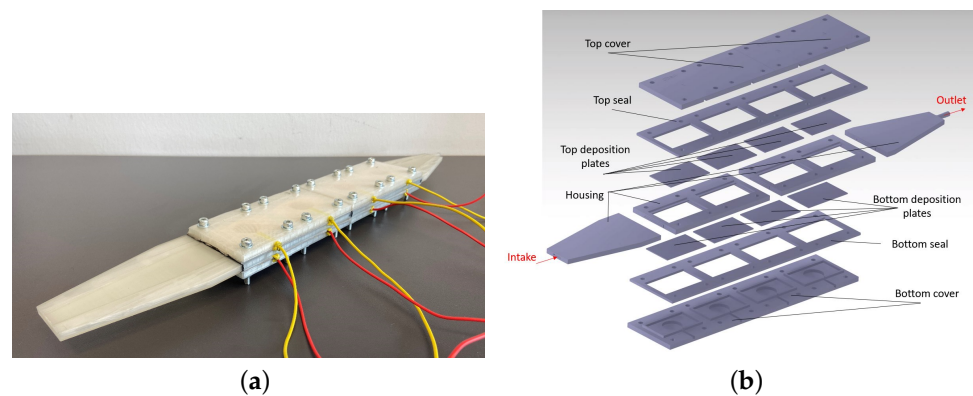


**Figure A1.** The custom-made electrostatic sampler. (a) A photograph of the custom-made electrostatic sampler. (b) CAD of the electrostatic sampler.

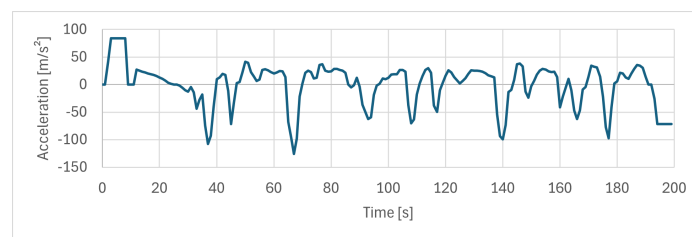
*Appendix A.2. Calculation*

The expected deposition size was calculated according to [35] and the manual of the TSI 3080 electrostatic classifier, assuming one charge per particle.

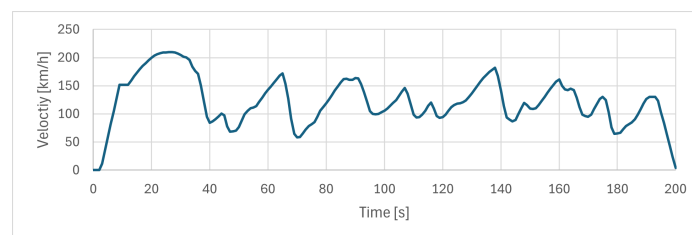
**Table A1.** Constants and parameters considered for the calculation.  $\alpha$ ,  $\beta$ , and  $\gamma$  are the factors used for the calculation of the Cunningham slip correction (CSP) factor.

	Value	Unit
Mean free path	$6.730 \times 10^{-8}$	m
Dynamic viscosity	$1.8325 \times 10^{-5}$	$\text{kg ms}^{-1}$
Air pressure	101.8	kPa
Temperature	310.15	K
$\alpha$ (CSP)	1.165	-
$\beta$ (CSP)	0.483	-
$\gamma$ (CSP)	0.997	-
Volume flow	1	$\text{L min}^{-1}$
Air permittivity	1.00059	$\text{As V}^{-1} \text{m}^{-1}$
Entry	Data	Data

**Appendix B. Drive Cycle**



(a)



(b)

**Figure A2.** Cont.

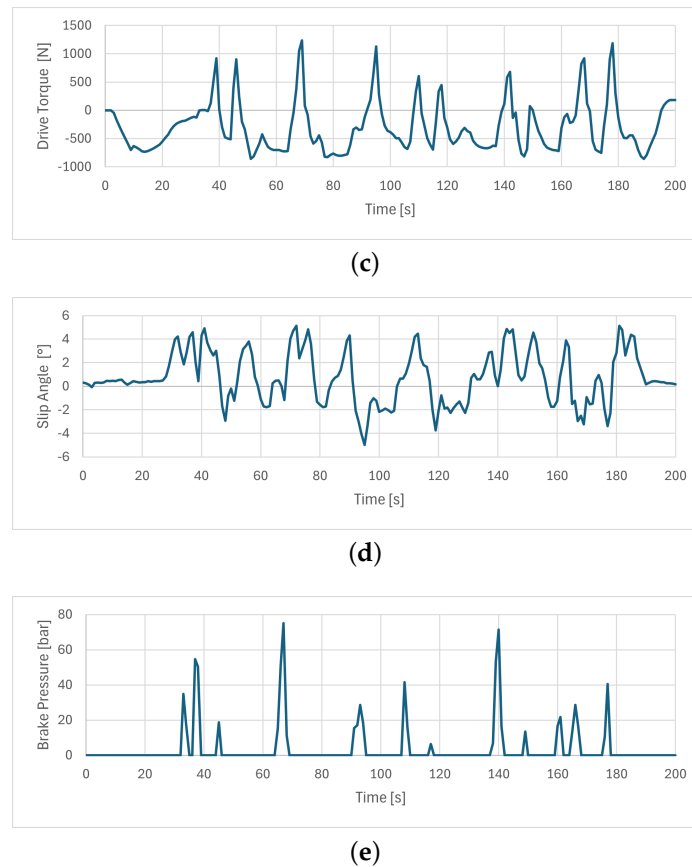


**Figure A2.** Selected time-dependent test-bed values set in the 200 s test cycle. The test cycle data are available upon request from the corresponding author. Acceleration was derived from the set velocity values. The parameters were harmonised, and deceleration was achieved through braking. (a) Acceleration—calculated from the velocity value. (b) Velocity. (c) Driving torque. (d) Slip angle. (e) Brake pressure.

**Appendix C. Particle Size Distributions in Absolute Concentrations**

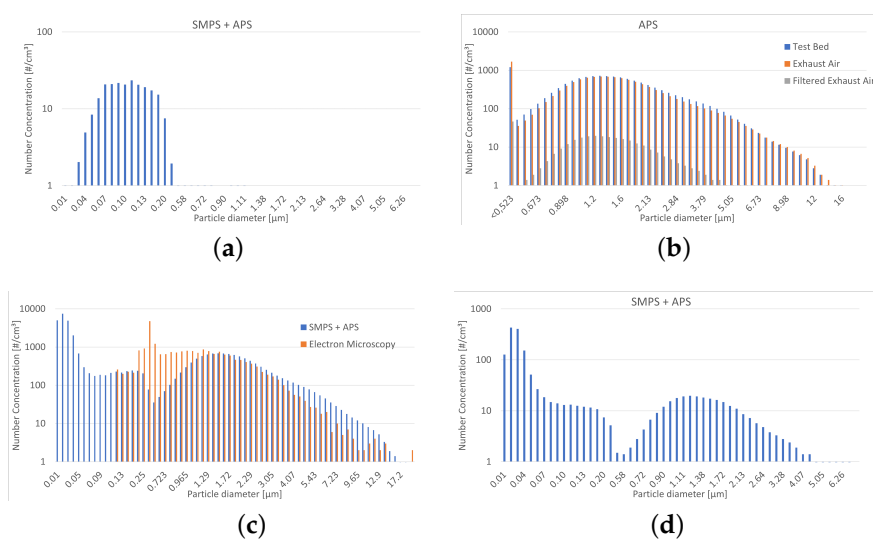


**Figure A3.** Plots of the raw PSD data for different sampling positions (see Figure 1b), measurements, and instruments for qualitative comparison. Different equivalent diameters were used for the different instruments. (a) PSDs measured in filtered supply air with the SMPS and APS. (b) A comparison of APS measurements for different sampling positions. (c) A comparison of PSDs measured in exhaust air with three different techniques. (d) PSDs measured in filtered exhaust air with the SMPS and APS.

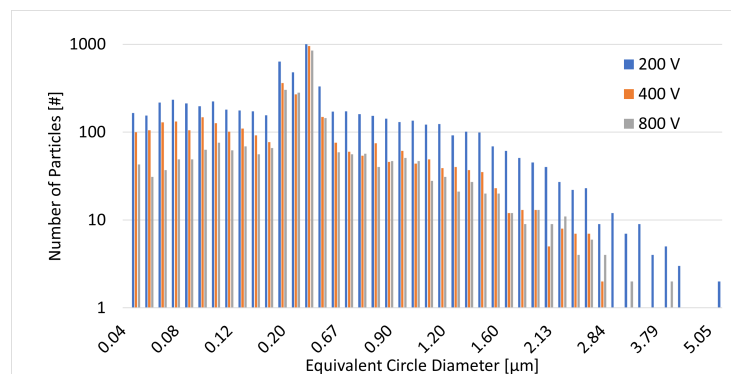


**Figure A4.** Obtained particle numbers at different ECDs in the single-particle analysis of the deposition plates. The PSD determined by EM single-particle analysis. Note that the  $y$ -axis is normalised; the figure with absolute concentrations can be found in Appendix C.

## References

- Sokhi, R.S.; Moussiopoulos, N.; Baklanov, A.; Bartzis, J.; Coll, I.; Finardi, S.; Friedrich, R.; Geels, C.; Grönholm, T.; Halenka, T.; et al. Advances in air quality research—Current and emerging challenges. *Atmos. Chem. Phys.* **2022**, *22*, 4615–4703. [CrossRef]
- European Environmental Agency. Air Quality in Europe 2022, Web Reprt. 2022. Available online: <https://www.eea.europa.eu/publications/air-quality-in-europe-2022> (accessed on 22 December 2023).
- Harrison, R.M.; Allan, J.; Carruthers, D.; Heal, M.R.; Lewis, A.C.; Marner, B.; Murrells, T.; Williams, A. Non-exhaust vehicle emissions of particulate matter and VOC from road traffic: A review. *Atmos. Environ.* **2021**, *262*, 118592. [CrossRef]
- Piscitello, A.; Bianco, C.; Casasso, A.; Sethi, R. Non-exhaust traffic emissions: Sources, characterization, and mitigation measures. *Sci. Total Environ.* **2021**, *766*, 144440. [CrossRef]
- Grigoratos, T.; Martini, G. Brake wear particle emissions: A review. *Environ. Sci. Pollut. Res.* **2015**, *22*, 2491–2504. [CrossRef]
- Stojanovic, N.; Glisovic, J.; Abdullah, O.I.; Belhocine, A.; Grujic, I. Particle formation due to brake wear, influence on the people health and measures for their reduction: A review. *Environ. Sci. Pollut. Res.* **2022**, *29*, 9606–9625. [CrossRef]
- Giechaskiel, B.; Grigoratos, T.; Mathissen, M.; Quik, J.; Tromp, P.; Gustafsson, M.; Franco, V.; Dilara, P. Contribution of Road Vehicle Tyre Wear to Microplastics and Ambient Air Pollution. *Sustainability* **2024**, *16*, 522. [CrossRef]
- Bondorf, L.; Köhler, L.; Grein, T.; Epple, F.; Philipps, F.; Aigner, M.; Schripp, T. Airborne Brake Wear Emissions from a Battery Electric Vehicle. *Atmosphere* **2023**, *14*, 488. [CrossRef]
- Dimopoulos Eggenschwiler, P.; Schreiber, D.; Habersatter, J. Brake Particle PN and PM Emissions of a Hybrid Light Duty Vehicle Measured on the Chassis Dynamometer. *Atmosphere* **2023**, *14*, 784. [CrossRef]
- Giechaskiel, B.; Grigoratos, T.; Dilara, P.; Karageorgiou, T.; Ntziachristos, L.; Samaras, Z. Light-Duty Vehicle Brake Emission Factors. *Atmosphere* **2024**, *15*, 97. [CrossRef]
- Council of the European Union. Press Release—Euro 7: Council and Parliament Strike Provisional Deal on Emissions Limits for Road Vehicles. 2023. Available online: <https://www.consilium.europa.eu/en/press/press-releases/2023/12/18/euro-7-council-and-parliament-strike-provisional-deal-on-emissions-limits-for-road-vehicles/#:~:text=With%20Euro%207%20we%20aim,zero%20emissions%20vehicles%20by%202035>. (accessed on 22 December 2023).
- Grigoratos, T.; Mathissen, M.; Vedula, R.T.; Mamakos, A.; Agudelo, C.; Gramstat, S.; Giechaskiel, B. Interlaboratory Study on Brake Particle Emissions—Part I: Particulate Matter Mass Emissions. *Atmosphere* **2023**, *14*, 498. [CrossRef]
- Mathissen, M.; Grigoratos, T.; Gramstat, S.; Mamakos, A.; Vedula, R.T.; Agudelo, C.; Grochowicz, J.; Giechaskiel, B. Interlaboratory Study on Brake Particle Emissions Part II: Particle Number Emissions. *Atmosphere* **2023**, *14*, 424. [CrossRef]
- Grigoratos, T.; Mamakos, A.; Arndt, M.; Lugovyy, D.; Anderson, R.; Hafenmayer, C.; Moisisio, M.; Vanhanen, J.; Frazee, R.; Agudelo, C.; et al. Characterization of Particle Number Setups for Measuring Brake Particle Emissions and Comparison with Exhaust Setups. *Atmosphere* **2023**, *14*, 103. [CrossRef]
- Giechaskiel, B.; Melas, A.; Martini, G.; Dilara, P.; Ntziachristos, L. Revisiting Total Particle Number Measurements for Vehicle Exhaust Regulations. *Atmosphere* **2022**, *13*, 155. [CrossRef]
- Mamakos, A.; Arndt, M.; Hesse, D.; Augsburg, K. Physical characterization of brake-wear particles in a PM10 dilution tunnel. *Atmosphere* **2019**, *10*, 639. [CrossRef]
- Farwick zum Hagen, F.H.; Mathissen, M.; Grabiec, T.; Hennicke, T.; Rettig, M.; Grochowicz, J.; Vogt, R.; Benter, T. On-road vehicle measurements of brake wear particle emissions. *Atmos. Environ.* **2019**, *217*, 116943. [CrossRef]
- Huber, M.P.; Fischer, P.; Murg, J.; Reingruber, H.; Wanek-Ruediger, C.; Weidinger, C.; Steiner, G. *Characterizing a Real-Driving Brake Emissions Sampling System on a Laboratory Test Bed*. SAE Technical Papers; SAE International: Warrendale PA, USA, 2023; pp. 1–13. [CrossRef]
- Huber, M.P.; Fischer, P.; Mamakos, A.; Steiner, G.; Klug, A. *Measuring Brake Wear Particles with a Real-Driving Emissions Sampling System on a Brake Dynamometer*. SAE Technical Papers; SAE International: Warrendale PA, USA, 2022; pp. 1–15. [CrossRef]

20. Fussell, J.C.; Franklin, M.; Green, D.C.; Gustafsson, M.; Harrison, R.M.; Hicks, W.; Kelly, F.J.; Kishta, F.; Miller, M.R.; Mudway, I.S.; et al. A Review of Road Traffic-Derived Non-Exhaust Particles: Emissions, Physicochemical Characteristics, Health Risks, and Mitigation Measures. *Environ. Sci. Technol.* **2022**, *56*, 6813–6835. [[CrossRef](#)]
21. Hesse, D.; Feißel, T.; Kunze, M.; Bachmann, E.; Bachmann, T.; Gramstat, S. Comparison of Methods for Sampling Particulate Emissions from Tires under Different Test Environments. *Atmosphere* **2022**, *13*, 1262. [[CrossRef](#)]
22. Schläfle, S.; Unrau, H.J.; Gauterin, F. Influence of Load Condition, Tire Type, and Ambient Temperature on the Emission of Tire–Road Particulate Matter. *Atmosphere* **2023**, *14*, 95. [[CrossRef](#)]
23. Grigoratos, T.; Gustafsson, M.; Eriksson, O.; Martini, G. Experimental investigation of tread wear and particle emission from tyres with different treadwear marking. *Atmos. Environ.* **2018**, *182*, 200–212. [[CrossRef](#)]
24. Giechaskiel, B.; Dilara, P.; Sandbach, E.; Andersson, J. Particle measurement programme (PMP) light-duty inter-laboratory exercise: Comparison of different particle number measurement systems. *Meas. Sci. Technol.* **2008**, *19*, 095401. [[CrossRef](#)]
25. Schurl, S.; Kupper, M.; Krassa, H.; Schmidt, S.; Sturm, S.; Heidinger, A. *A PN-Measurement System for Small Engine Applications*. SAE Technical Papers; SAE International: Warrendale PA, USA, 2023; pp. 1–7. [[CrossRef](#)]
26. Giechaskiel, B.; Wang, X.; Gilliland, D.; Drossinos, Y. The effect of particle chemical composition on the activation probability in n-butanol condensation particle counters. *J. Aerosol Sci.* **2011**, *42*, 20–37. [[CrossRef](#)]
27. Wlasits, P.J.; Stolzenburg, D.; Tauber, C.; Brilke, S.; Schmitt, S.H.; Winkler, P.M.; Wimmer, D. Counting on chemistry: Laboratory evaluation of seed-material-dependent detection efficiencies of ultrafine condensation particle counters. *Atmos. Meas. Tech.* **2020**, *13*, 3787–3798. [[CrossRef](#)]
28. Krassa, H.; Kupper, M.; Schriefl, M.A.; Bergmann, A. Toward a simplified calibration method for 23 nm automotive particle counters using atomized inorganic salt particles. *Aerosol Sci. Technol.* **2023**, *57*, 329–341. [[CrossRef](#)]
29. Gasser, E. Characterization of Gas and Particle Released during Thermal Runaway of Li-Ion Batteries. Master’s Thesis, Graz University of Technology, Graz, Austria, 2019; pp. 2–92.
30. Asbach, C.; Todea, A.M.; Zessinger, M.; Kaminski, H. *Entstehung und Möglichkeiten zur Messung von Fein- und Ultrafeinstaub beim Bremsen*; Springer Vieweg: Berlin/Heidelberg, Germany, 2019; pp. 45–67. [[CrossRef](#)]
31. Oroumijeh, F.; Zhu, Y. Brake and tire particles measured from on-road vehicles: Effects of vehicle mass and braking intensity. *Atmos. Environ. X* **2021**, *12*, 100121. [[CrossRef](#)]
32. Mathissen, M.; Grochowicz, J.; Schmidt, C.; Vogt, R.; Farwick zum Hagen, F.H.; Grabiec, T.; Steven, H.; Grigoratos, T. A novel real-world braking cycle for studying brake wear particle emissions. *Wear* **2018**, *414–415*, 219–226. [[CrossRef](#)]
33. Wang, Y.; Yin, H.; Yang, Z.; Su, S.; Hao, L.; Tan, J.; Wang, X.; Niu, Z.; Ge, Y. Assessing the brake particle emissions for sustainable transport: A review. *Renew. Sustain. Energy Rev.* **2022**, *167*, 112737. [[CrossRef](#)]
34. Mamakos, A.; Huber, M.P.; Arndt, M.; Reingruber, H.; Steiner, G.; Weidinger, C. *Design of a Laboratory Sampling System for Brake Wear Particle Measurements*. SAE Technical Papers; SAE International: Warrendale PA, USA, 2022; Volume 1, pp. 1–11. [[CrossRef](#)]
35. Bilby, D.; Kubinski, D.J.; Maricq, M.M. Current amplification in an electrostatic trap by soot dendrite growth and fragmentation: Application to soot sensors. *J. Aerosol Sci.* **2015**, *98*, 41–58. [[CrossRef](#)]

**Disclaimer/Publisher’s Note:** The statements, opinions and data contained in all publications are solely those of the individual author(s) and contributor(s) and not of MDPI and/or the editor(s). MDPI and/or the editor(s) disclaim responsibility for any injury to people or property resulting from any ideas, methods, instructions or products referred to in the content.